# Influence of thermomagnetic convection and ferrofluid thermophysical properties on heat transfers in a cylindrical container heated by a solenoid

Raphael Zanella, Caroline Nore, Frédéric Bouillault, Jean-Luc Guermond, Xavier Mininger

# Influence of thermomagnetic convection and ferrofluid thermophysical properties on heat transfers in a cylindrical container heated by a solenoid

Raphaël Zanella[a,b,c,*], Caroline Nore[a], Frédéric Bouillault[b], Jean-Luc Guermond[c], Xavier Mininger[b]

[a] *LIMSI, CNRS, Univ. Paris-Sud, Université Paris-Saclay, F-91405 Orsay, France*
[b] *GeePs, CNRS / CentraleSupélec - UPMC - UPSud, 91192 Gif sur Yvette cedex, France*
[c] *Department of Mathematics, Texas A&M University, College Station, TX 77843 USA*

**Abstract**

The thermal convection in a cylindrical container heated by a solenoid and cooled with an oil-based ferrofluid is numerically studied. The temperature and the velocity fields are compared to those obtained with pure oil to assess the benefits of using ferrofluids for cooling systems like electrical transformers. The influence of the magnetic body force on the flow and the temperature in the system is investigated in various configurations. One original result established in this paper is that the changes in the fluid properties due to the presence of nanoparticles, such as viscosity and thermal conductivity, have a significant impact on the heat transfers. A second result is that the use of a ferromagnetic core enhances the cooling.

*Keywords:* Ferrofluid, Natural convection, Thermomagnetic convection, Finite element method, Power transformer

## 1. Introduction

Ferrofluids are suspensions of magnetic nanoparticles in a liquid carrier. Thermal agitation and the addition of a surfactant prevent sedimentation and aggregation of the nanoparticles. If well prepared, the suspension stays stable even under the action of a magnetic field. It is common to use the continuum hypothesis to model ferrofluids. In the presence of a magnetic field, the nanoparticles generate a body force that depends on the gradient of the amplitude of the magnetic field. Among the various models for this effect that are available in the literature, we are going to consider in this paper the so-called Kelvin

[☆] Fully documented templates are available in the elsarticle package on CTAN.

[*] Corresponding author
*Email address:* zanella@limsi.fr (Raphaël Zanella)

body force model ($N/m^3$):

$$\mathbf{F} = \mu_0(\mathbf{M}\cdot\nabla)\mathbf{H}, \tag{1}$$

where $\mu_0$ is the magnetic permeability of vacuum, $\mathbf{M}$ is the ferrofluid magnetization, and $\mathbf{H}$ is the magnetic field. This body force model is dominant in the literature on ferrofluid modeling, see [1, 2, 3, 4, 5] for instance. Since magnetization decreases with the temperature due to the thermal agitation of the magnetic dipoles of the nanoparticles, temperature gradients generate spatial variations of the magnetic body force. This force is stronger in cold regions than in hot regions. If the magnetic field source is close to the heat source [6], the spatial variations of the magnetic body force lead to a global motion called thermomagnetic convection.

The magnetic nanoparticles, generally composed of metallic material, do not only cause thermomagnetic convection, they also affect the properties of the fluid. The density, the heat capacity, the thermal conductivity, the thermal expansion, and the viscosity of the ferrofluid, seen as an homogeneous medium, are different from that of the base fluid [7, 8]. These changes of properties may have antagonizing effects on the cooling performance of ferrofluids. For example, while the increase of thermal conductivity improves the heat transfer rate, the increase of viscosity slows down the flow and therefore may reduce heat transfers. It is thus unclear whether using ferrofluid for cooling purpose is beneficial or not, [9].

The goal of the present work is to investigate the use of ferrofluids for the cooling of electromagnetic systems, such as power transformers. If the heat transfer rate can be increased in these devices by using ferrofluids, the volume of cooling fluid could be either reduced or mechanical cooling systems could be avoided. Early experiments on small distribution transformers using either a ferrofluid or a pure transformer oil as cooling agent show that the overall temperature is lower in the ferrofluid setup [10]. It is also observed in [11] that heat transfers are enhanced by using ferrofluid instead of regular oil to cool an immersed coil. Encouraging numerical simulations of a transformer prototype are reported in [12]: a strong temperature reduction is observed when using a ferrofluid. Experimental works on a transformer prototype [13, 14] also show the benefit of ferrofluid as coolant: the temperature at hot-spots is significantly lowered. The temperature of an immersed coil is numerically shown to be lower when using ferrofluid in [15], but this result is only theoretical since the impact of the nanoparticles on the physical properties was not taken into account.

The aim of the present paper is to understand the influence on heat transfers of both the thermomagnetic convection and the modifications of the fluid properties due to the presence of magnetic nanoparticles. An immersed coil system, close to that of [11], is simulated with the SFEMaNS code [16]. The thermo-hydrodynamical model is first validated against an experiment on pure transformer oil. The temperature and velocity fields obtained with transformer oil and transformer oil-based ferrofluid are then compared to assess and understand the benefit of using ferrofluids. An iron core is added to observe the effect

of a piece of ferromagnetic material representing the magnetic core of an electrical transformer. Classical models for the properties of the ferrofluid taking into account the volume fraction of magnetic nanoparticles are used. The ferrofluid magnetization follows an approximation of Langevin's law, generally considered in the literature to be an appropriate model of the paramagnetic behavior. This model naturally includes the temperature dependence [17].

## 2. Material and methods

### *2.1. Problem description*

We consider an electromagnetic system constituted of a copper coil immersed in a ferrofluid composed of transformer oil with magnetite nanoparticles in small concentration. The ferrofluid is enclosed in an aluminium container. A magnetic field is produced by a DC current flowing through the coil. The heat source is the Joule effect in the coil. The action of the magnetic field combined with the heat flux generates thermomagnetic convection [6]. This setup is a simplified model of an electrical transformer. In the present paper we present numerical simulations and experimental results on this configuration.

| Parameter | $H_t$ | $R_t$ | $e_{w1}$ | $e_{w2}$ | $e_{w3}$ | $H_0$ |
|---|---|---|---|---|---|---|
| Value (cm) | 12.5 | 3.1 | 1 | 2 | 1 | 3.9 |
| Parameter | $L_0$ | $R_i$ | $R_e$ | $R_c$ | $e_{c1}$ | $e_{c2}$ |
| Value (cm) | 2.1 | 0.8 | 1.175 | 2.6 | 2 | 1 |

Table 1: Dimensions of the experimental setup.

Fig. 1 shows the setup that is used for the experiment and a first series of numerical simulations; the dimensions are reported in Tab. 1. The cap is made of PVC to avoid short circuits. The positions of the thermal sensors are indicated by crosses. Fig. 2 shows two other configurations that are used only for numerical simulations whose purpose is to test the ferrofluid effects. In the first configuration (left panel) there is no ferromagnetic core at the center of the coil, whereas there is one in the second configuration (right panel). In both cases, the dimensions of the coil and the container are the same as those in Fig. 1. The temperature is monitored in the coil in a region where the temperature is close to being maximal; this point is indicated by a cross. The cap of the container is made of aluminium. We have verified numerically that whether the cap is made of PVC or aluminium does not change significantly the temperature distribution. We have chosen to report the numerical results obtained with an aluminium cap since it may better represent an actual transformer.

### *2.2. Governing equations*

In this paper we only consider weakly concentrated ferrofluids (volume fraction of nanoparticles $\phi \leq 7\%$) which, as reported in the abundant literature on the topic, are well described by using the homogeneous fluid hypothesis. The

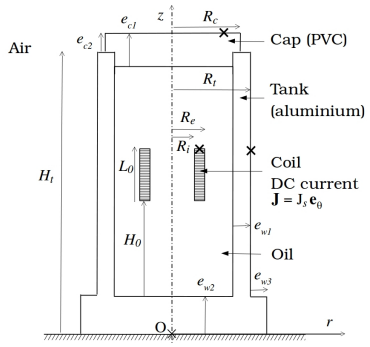


Figure 1: Setup using pure transformer oil (experiment and numerical simulations). The cross marks show the three thermal sensors used to monitor the temperature.

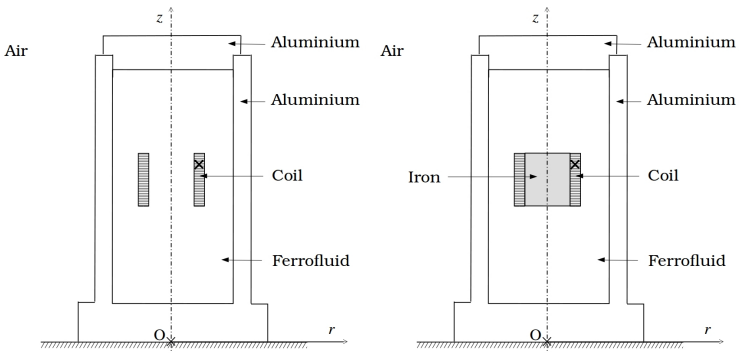


(a) Without core (b) With core

Figure 2: Setups used for numerical simulations with ferrofluid. The cross marks show the points where the temperature is monitored ($r = 1$ cm, $z = 7.5$ cm).

magnetostatic approximation for electromagnetism is used in the solids and in the fluid; the equations are

$$\nabla \times \mathbf{H} = \mathbf{J}, \tag{2}$$

$$\nabla \cdot (\mu \mathbf{H}) = 0, \tag{3}$$

where $\mathbf{H}$ is the magnetic field, $\mathbf{J}$ is the current density, equal to $J_s \mathbf{e}_\theta = \frac{NI}{S} \mathbf{e}_\theta$ in the coil and zero elsewhere ($N$ is the number of windings, $I$ is the enforced current and $S$ is the section of the coil body), and $\mu$ is the magnetic permeability. The motion of the fluid is modeled by the incompressible Navier-Stokes equations:

$$\rho \partial_t \mathbf{u} + \rho (\mathbf{u} \cdot \nabla) \mathbf{u} + \nabla p - \nabla \cdot (\eta(T) \nabla^s \mathbf{u}) = \alpha \rho g (T - T_0) \mathbf{e}_z + \mu_0 M(T) \nabla H, \tag{4}$$

$$\nabla \cdot \mathbf{u} = 0, \tag{5}$$

where $\mathbf{u}$ is the velocity, $p$ is the pressure, $T$ is the temperature, $T_0$ is the exterior temperature, $\rho$ is the density, $\eta$ is the dynamic viscosity and $\alpha$ is the thermal

expansion. Here we use the notation $\nabla^s \mathbf{u} = \frac{1}{2}(\nabla \mathbf{u} + (\nabla \mathbf{u})^\mathsf{T})$. The buoyancy effects are modeled by using the Boussinesq approximation. The last term on the right-hand side is the simplified expression of the Kelvin body force given in Eq. (1) with the convention $M = \|\mathbf{M}\|$ and $H = \|\mathbf{H}\|$; this expression is obtained by assuming that ferrofluid magnetization $\mathbf{M}$ is instantaneously aligned with the magnetic field $\mathbf{H}$ and $\nabla \times \mathbf{H} = \mathbf{0}$ in the fluid, [1]. The conservation of energy is modeled as follows:

$$\rho c \partial_t T + \rho c (\mathbf{u} \cdot \nabla) T - \nabla \cdot (\lambda \nabla T) = f_T, \tag{6}$$

where $c$ is the specific heat capacity, $\lambda$ is the thermal conductivity, and $f_T$ is the heat source, equal to the Joule effect $\frac{RI^2}{V}$ in the coil and zero elsewhere ($R$ is the electrical resistance of the wire and $V$ is the volume of the coil body). The energy production by viscous dissipation is neglected.

The boundary condition for the magnetic problem $\mathbf{H} \times \mathbf{n} = \mathbf{0}$ is enforced at the exterior boundary of the tank and the cap. The non-slip boundary condition $\mathbf{u} = \mathbf{0}$ is applied at the boundary of the fluid domain. The air convection at the top and on the lateral wall of the container is modeled by using a Robin boundary condition on the temperature:

$$-\lambda \nabla T \cdot \mathbf{n} = h(T - T_0), \tag{7}$$

where $h$ is the convection coefficient and $\mathbf{n}$ is the outer unit normal vector. The homogeneous Neumann boundary condition $\partial_z T = 0$ is enforced at the bottom of the tank. The initial conditions are $\mathbf{u} = \mathbf{0}$, $T = T_0$, and $\mathbf{H} = \mathbf{0}$.

### *2.3. Ferrofluid modeling*

We assume that the magnetization intensity is proportional to the magnetic field intensity, and the proportionality constant depends on the temperature:

$$M = \chi(T) H, \tag{8}$$

with $\chi$ the susceptibility given by an approximation of Langevin's law [17]:

$$\chi(T) = \frac{\phi \mu_0 \pi d^3 M_0^2}{18 k_B T}, \tag{9}$$

where $\phi$ is the volume fraction of magnetic material, $d$ is the particle diameter, $M_0$ is the particle magnetization, and $k_B$ is the Boltzmann constant. Notice that in the present setting, it is essential that $\chi$ depends on the temperature for the Kelvin force to be active. If $\chi$ is constant, then $\mu_0 M(T) \nabla H = \mu_0 \chi \nabla \frac{1}{2} H^2$, and the Kelvin force in Eq. (4) is just an hydrostatic pressure, which cannot generate any motion. But, when $\chi$ depends on $T$, the gradient of magnetization in the ferrofluid due to the evolution of the temperature leads to a gradient of the magnetic body force in Eq. (4), which generates thermomagnetic convection. In Eq. (3), the magnetic permeability $\mu$ is defined to be a piecewise constant. It is equal to $\mu_0(1 + \chi(T_0))$ in the ferrofluid.

The properties of the ferrofluid are obtained from the properties of the transformer oil and the magnetite of the nanoparticles. The density and the specific heat capacity are determined from a mixture law relative to the volume fraction of magnetic material $\phi$:

$$\rho_{\mathrm{ff}} = \phi\rho_{\mathrm{p}} + (1-\phi)\rho_{\mathrm{bf}}, \tag{10}$$

$$\rho_{\mathrm{ff}} c_{\mathrm{ff}} = (1-\phi)\rho_{\mathrm{bf}} c_{\mathrm{bf}} + \phi\rho_{\mathrm{p}} c_{\mathrm{p}}, \tag{11}$$

where the subscripts "ff", "bf" and "p" refer to the ferrofluid, the base fluid and the nanoparticles respectively.

The thermal conductivity is described by the classical model of Maxwell for nanofluids [18, 19]:

$$\lambda_{\mathrm{ff}} = \frac{1+2\beta\phi}{1-\beta\phi}\lambda_{\mathrm{bf}}, \qquad \beta = \frac{\lambda_{\mathrm{p}} - \lambda_{\mathrm{bf}}}{\lambda_{\mathrm{p}} + 2\lambda_{\mathrm{bf}}}. \tag{12}$$

To avoid sedimentation and aggregation of the nanoparticles, the particles are coated with surfactant. This coating changes some physical properties of the fluid, and this effect is modeled by introducing a second volume fraction, $\tilde{\phi}$, that accounts for the presence of the surfactant. The nanoparticles are supposed to have a diameter $d = 10$ nm and the surfactant thickness is supposed to be $s = 2$ nm. The volume fraction of the nanoparticles free of surfactant and the volume fraction of the nanoparticles when coated with surfactant are related through the following expression:

$$\tilde{\phi} = \left(1 + \frac{2s}{d}\right)\phi. \tag{13}$$

The dynamic viscosity is based on Rosensweig's model [8]:

$$\eta_{\mathrm{ff}} = \left(1 - \frac{5}{2}\tilde{\phi} + \frac{\frac{5}{2}\tilde{\phi}_c - 1}{\tilde{\phi}_c^2}\tilde{\phi}^2\right)^{-1} \eta_{\mathrm{bf}}. \tag{14}$$

with $\tilde{\phi}_c = 0.74$. The thermal expansion of the magnetic material and the surfactant is neglected and the thermal expansion of the ferrofluid is thus defined by

$$\alpha_{\mathrm{ff}} = (1-\tilde{\phi})\alpha_{\mathrm{bf}}. \tag{15}$$

### *2.4. Solid parts modeling*

The magnetic permeability $\mu$ is equal to $\mu_0$ in the cap, the container walls, and the coil. Based on the dimensions of the coil body, the wire and the number of windings, we estimate that the copper represents $\phi_{\mathrm{Cu}} = 37\%$ of the volume of the coil body. To account for the presence of oil within the coil body, the properties of the coil are homogenized in the numerical simulations by using the expressions:

$$\rho_{\mathrm{coil}} = \phi_{\mathrm{Cu}}\rho_{\mathrm{Cu}} + (1-\phi_{\mathrm{Cu}})\rho_{\mathrm{xx}}, \tag{16}$$

$$\rho_{\mathrm{coil}} c_{\mathrm{coil}} = \phi_{\mathrm{Cu}}\rho_{\mathrm{Cu}} c_{\mathrm{Cu}} + (1-\phi_{\mathrm{Cu}})\rho_{\mathrm{xx}} c_{\mathrm{xx}}, \tag{17}$$

where the index xx must be replaced by either bf or ff depending on the configuration considered. The thermal conductivity is given by the analytical law developed in [20, Eq. (12)-(13)]:

$$\frac{\lambda_{\mathrm{coil}}}{\lambda_{\mathrm{xx}}} = 1 - 2\phi_{\mathrm{Cu}} \left( \Lambda + \phi_{\mathrm{Cu}} - \frac{0.075422\,\phi_{\mathrm{Cu}}^{6}\Lambda}{\Lambda^2 - 1.060283\,\phi_{\mathrm{Cu}}^{12}} - \frac{0.000076\,\phi_{\mathrm{Cu}}^{12}}{\Lambda} \right)^{-1}, \quad (18)$$

$$\Lambda = \left(1 + \frac{\lambda_{\mathrm{Cu}}}{\lambda_{\mathrm{xx}}}\right) \left(1 - \frac{\lambda_{\mathrm{Cu}}}{\lambda_{\mathrm{xx}}}\right)^{-1}, \quad (19)$$

where $\lambda_{\mathrm{xx}}$ is either $\lambda_{\mathrm{bf}}$ or $\lambda_{\mathrm{ff}}$ depending on the configuration considered. This approach is used in [15] in a similar case.

*2.5. Physical properties*

The number of windings is $N = 33$. The electrical resistance of the wire is $R = 47$ m$\Omega$. The current flowing in the wire is $I = 12$ A.

The transformer oil used in the experiment is the vegetable oil eN 1215. The dynamic viscosity strongly varies with the temperature and is approximated by using the expression:

$$\eta(T) = A \exp\left(\frac{B}{T}\right), \quad (20)$$

with $A \simeq 1.3 \times 10^{-6}$ Pa·s, $B \simeq 3.1 \times 10^{3}$ K and $T$ in K. The comparison between the model (20) and the manufacturer's data is presented in Fig. 3. Since the dependence of the other fluid properties (density, thermal expansion, specific heat capacity, and thermal conductivity) with respect to the temperature is small over the temperature range considered in this work, the said fluid properties are assumed to be constant and are equal to their value at 20 °C. The properties of the different materials used in this work are presented in Tab. 2.

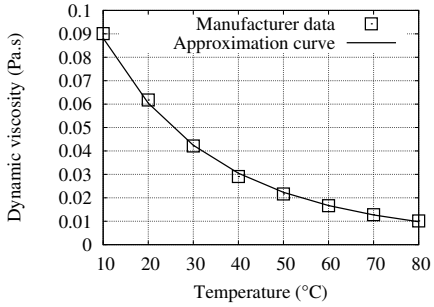


Figure 3: Dynamic viscosity of the vegetable oil eN 1215 with respect to temperature and approximation (20).

The magnetization of the magnetite is $M_0 = 446$ kA/m and the relative magnetic permeability of the iron core is taken equal to 1000.

| Property | Copper | Oil | Aluminum | PVC | Iron | Magnetite |
|---|---|---|---|---|---|---|
| Density (kg/m$^3$) | 8933 | 922 | 2.70e3 | 1.4e3 | 7870 | 5.18e3 |
| Thermal expansion (/K) | - | 7.4e-4 | - | - | - | |
| Heat capacity (J/K·kg) | 385 | 1970 | 945 | 1e3 | 447 | 630 |
| Therm. cond. (W/m·K) | 401 | 0.166 | 201 | 0.16 | 80.2 | 6 |

Table 2: Properties used in the simulations.

## 3. Computational details

### *3.1. Numerical method*

The numerical simulations are done with the magnetohydrodynamics code called SFEMaNS (see [16]). The approximation in space uses Fourier expansions and finite elements. The method is based on cylindrical coordinates, and every field $f$ is solved as a partial Fourier sum relative to the azimuthal direction

$$f(r,\theta,z) = \sum_{m=0}^{m_{\max}} f_m^c(r,z)\cos(m\theta) + \sum_{m=1}^{m_{\max}} f_m^s(r,z)\sin(m\theta), \tag{21}$$

where $m_{\max}$ is the maximum number of complex Fourier modes. The Fourier coefficients $f_m^c(r,z)$ and $f_m^s(r,z)$ are approximated by using Lagrange finite elements in the meridian section. Once the nonlinear terms are made explicit in Eq. (4)-(6), all the Fourier coefficients can be solved independently in parallel. The nonlinear terms are computed by using a parallelized version of FFT3W. The linear algebra for each Fourier coefficient is done in parallel by using subroutines from the portable extensible toolkit for scientific computation library (PETSc) [21]. In conclusion, the SFEMaNS code is parallelized in the Fourier direction and in each meridian section.

Quadratic, $\mathbb{P}_2$, continuous Lagrange elements are used for the temperature and the velocity and linear, $\mathbb{P}_1$, continuous Lagrange elements are used for the pressure to ensure the inf-sup condition. The magnetic field is approximated by using quadratic continuous Lagrange elements, with a technique to enforce $\nabla\cdot(\mu\mathbf{H}) = 0$ based on a penalty method. The coupling across the axisymmetric interfaces of discontinuous electric conductivity or magnetic permeability is enforced by an interior penalty method. SFEMaNS has been thoroughly validated on numerous analytical solutions and against other magnetohydrodynamics codes [16, 22, 23, 24].

The equations considered in this paper are solved according to the flowchart shown in Fig. 4. All the computations reported in this paper are done assuming axisymmetry, i.e., $m_{\max} = 0$. We have done various computations with $m_{\max} > 0$ (not reported here) and observed that the solution is axisymmetric in the conditions considered here.

### *3.2. Finite element meshes*

The numerical simulations reported in this paper are done with two different meridian meshes. For the simulations in the configuration without core, the

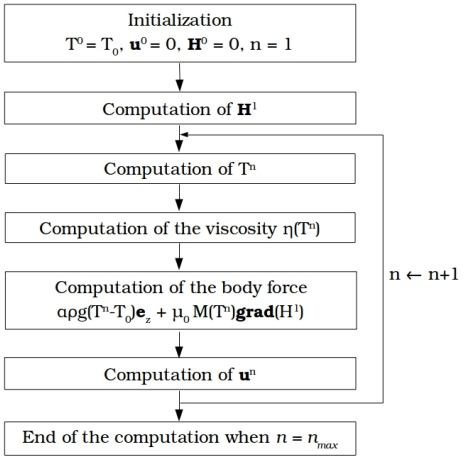


Figure 4: Flowchart of the method; $n_{\max}$ is the maximum number of iterations. Due to the DC current, the magnetic field is computed only once.

mesh is composed of 3786 $\mathbb{P}_1$ nodes and 14048 $\mathbb{P}_2$ nodes. The mesh for the configuration with a core is composed of 4723 $\mathbb{P}_1$ nodes and 17762 $\mathbb{P}_2$ nodes. The mesh size goes from 0.04 cm in the coil and close to the core boundary to 0.15 cm at the exterior boundary of the container, see Fig. 5.

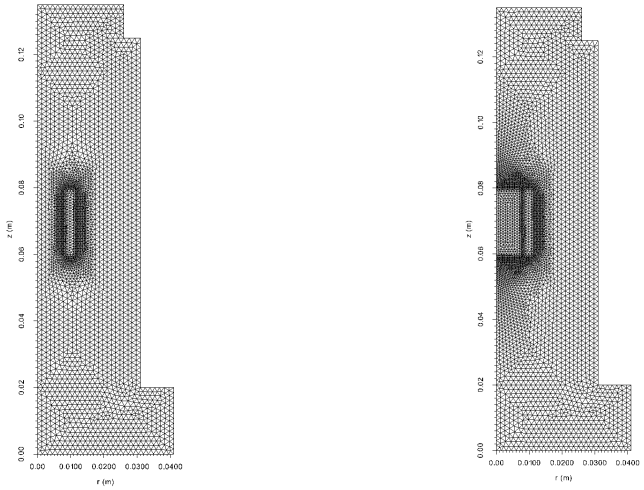

Figure 5: Finite element $\mathbb{P}_1$ meshes. Left: without core; Right: with core.

In order to test the accuracy of the method we have done computations with various meshsizes. We show in Fig. 6 two series of computations: one is done on the configuration with pure transformer oil and without the core using the mesh composed of 3786 $\mathbb{P}_1$ nodes and 14048 $\mathbb{P}_2$ nodes, the other series is done on the refined mesh obtained from the previous one by dividing each triangle into four

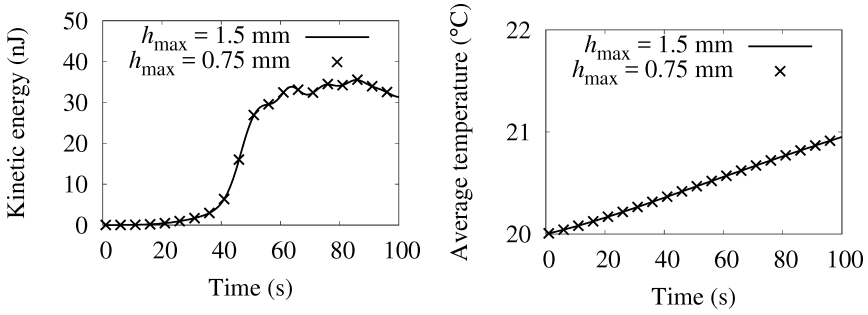


Figure 6: Grid dependence test.

new triangles. The global kinetic energy and the $L^2$-norm of the temperature are shown as functions of time for the two meshes. We observe that refining the mesh does not bring any significant change to the results, thereby showing that the approximation error is negligible for any practical purpose.

## 4. Experiment vs. numerics using pure transformer oil

Here, the thermo-hydrodynamical model is validated against experimental data obtained using pure transformer oil. The Kelvin force is zero in this case. We show in Fig. 7 the time evolution of the temperature for the three thermal sensors, see Fig. 1. The convection coefficient $h = 8$ W/m$^2$·K has been optimized to match this experiment and is within the typical range often reported in the literature, [25]. We have observed in the numerical simulations that the oscillations that are visible at the coil sensor are due to an unstable plume of hot fluid flowing up from the coil to the top wall. The period is about 6s. The numerical results are close to the experimental ones, and the thermo-hydrodynamical model is thus validated.

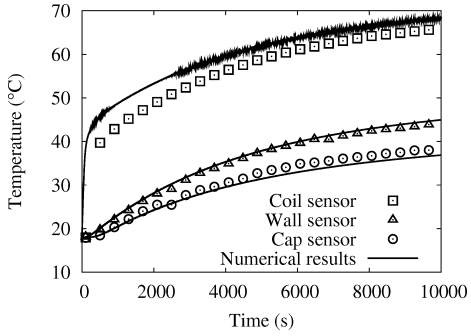


Figure 7: Comparison of the numerical results with the experimental data using pure transformer oil.

## 5. Numerical simulations with ferrofluid

In this section we report on numerical simulations done with ferrofluids. As previously explained, the properties of the fluid are changed due to the presence of the nanoparticles and an additional (magnetic) body force is present in the momentum equations. Five volume fractions of nanoparticles $\phi$ are tested: 0 (pure oil), 1, 3, 5 and 7%.

### *5.1. Influence of $\phi$ on the temperature*

Fig. 8 shows the time evolution of the temperature at a point in the coil where the temperature is close to being the highest. The results for the volume fractions 0, 1, 3, 5 and 7% are reported. The results in the left panel have been obtained for the configuration without core, and the results in the right panel have been obtained for the configuration with a ferromagnetic core. We observe that, for all the volume fractions considered, the higher the volume fraction, the lower the temperature over the entire time range. In the absence of core, the temperature difference between $\phi = 0$ and $\phi = 7\%$ is approximately 4°C at $t = 10000$ s. In the presence of the ferromagnetic core, this temperature difference is approximately 13°C. These simulations show that the heat transfer rate is improved when using ferrofluid instead of regular oil. This temperature difference is the highest when there is a ferromagnetic core.

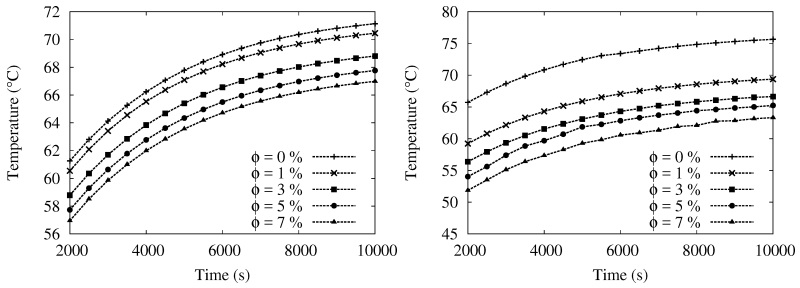


Figure 8: Time evolution of the temperature at the hot spot for various volume fractions of nanoparticles. Left: Without core; Right: With core.

### *5.2. Compared influence of physical properties and the Kelvin force*

In order to compare the effect of the Kelvin force with the changes of physical properties due to the presence of the nanoparticles, we now perform computations with the ferrofluid but with the Kelvin force being switched off. The results are reported in Fig. 9 (no core) and Fig. 10 (core). In each graph, we show again the time evolution obtained with $\phi = 0$ and $\phi \neq 0$ with the Kelvin force being active, and we report also the time evolution obtained with $\phi \neq 0$ and the Kelvin force being switched off. In the absence of core, the effects of the changes in the physical properties are of the same order as that of the Kelvin force. For instance, with $\phi = 7$ % and at $t = 10000$ s, the change in physical

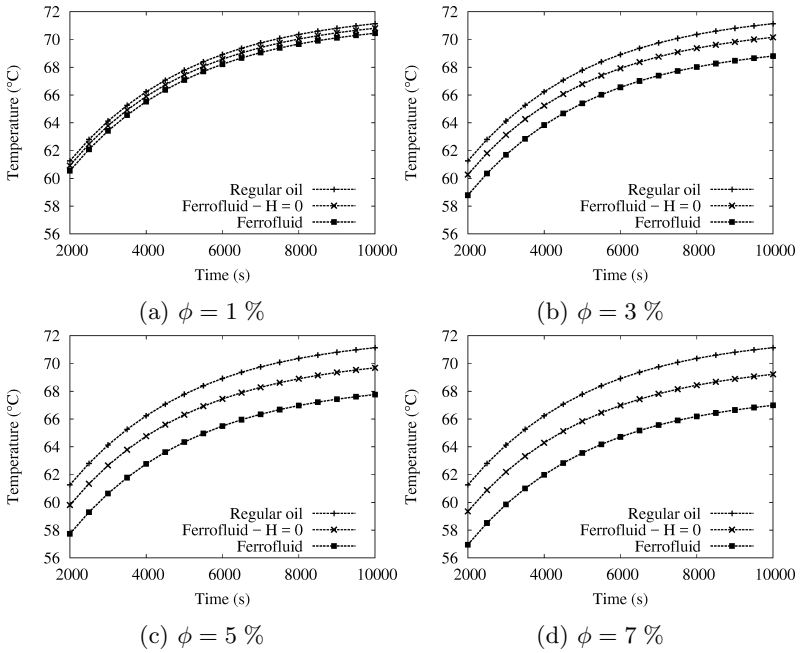


(a) $\phi = 1$ %

(b) $\phi = 3$ %

(c) $\phi = 5$ %

(d) $\phi = 7$ %

Figure 9: Setup without ferromagnetic core. Time evolution of the temperature at the hot spot with and without the Kelvin force.

properties reduces the temperature by 2°C approximately and the Kelvin force further reduces the temperature by 2°C.

When there is a ferromagnetic core, the effects due to the changes in physical properties are small compared to the effects of the Kelvin force. For instance, for $\phi = 7\%$, at $t = 10000$s, the changes of the physical properties reduce the temperature by 3°C approximately, and the Kelvin force further reduces the temperature by 10°C.

In conclusion, the numerical simulations reported in this section show that the changes in physical properties can affect the temperature of the system in a non negligible manner, and in some cases can be of the same order as the effects of the Kelvin force.

### *5.3. Temperature and velocity fields with and without Kelvin force*

In this section we fix $\phi = 7\%$, and we compare the temperature and velocity fields in the meridian section at $t = 10000$s in the same configurations as in §5.2; namely, $\phi = 0$, $\phi = 7\%$ without the Kelvin force, and $\phi = 7\%$ with the Kelvin force.

We show in Fig. 11 and Fig. 12 the temperature and the velocity fields obtained in the configuration without ferromagnetic core. We observe the same behavior on the temperature field as that reported in §5.2 for the hot spot. The temperature decrease induced by the Kelvin force has its origin in the change

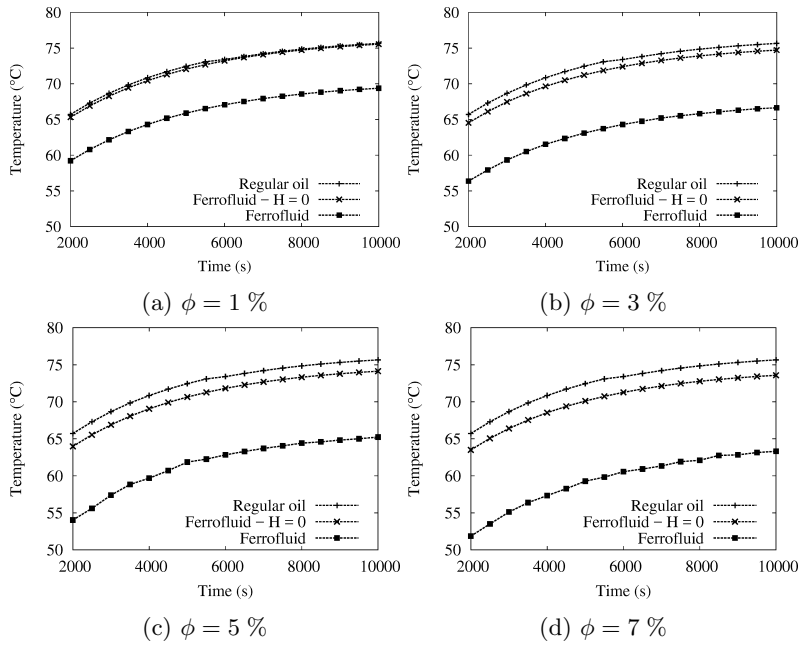


Figure 10: Setup with ferromagnetic core. Time evolution of the temperature at the hot spot with and without the Kelvin force.

in the convection pattern. The convection cells in the panels 12a and 12b are similar but are clearly different from that in panel 12c. In this panel, we observe that the Kelvin force generates a second convection cell inside the coil, close to the bottom of the coil. The modifications of the flow induced by the Kelvin force strengthens the heat transfer rate.

The same types of results are presented in Fig. 13 and Fig. 14 for the configuration with the ferromagnetic core. Again, the maximum temperature in the system is reduced when the pure oil is replaced by ferrofluid and with the Kelvin force switched off (from 77.63°C to 75.3°C). The action of the Kelvin force makes the convection more vigorous and the cooling is consequently more efficient (from 75.3°C to 64.4°C). The temperature drop due to the Kelvin force is more pronounced here (10.9°C with the core, 2.2°C without the core). Notice that for pure transformer oil the maximum temperature is larger in the configuration with the ferromagnetic core than in the configuration without the core (71.2°C without the core, 77.6°C with the core). This effect is reversed with the ferrofluid ($\phi = 7\%$); the maximum temperature decreases from 67.1°C without the core to 64.4°C with the core. The core has thus a negative impact when using pure transformer oil and a positive one when using ferrofluid. The velocity field is strongly modified by the presence of the core; the core blocks the upward flow along the axis, see Fig. 14c. Notice that when the Kelvin force is active there are recirculation cells at the top and at the bottom of the core;

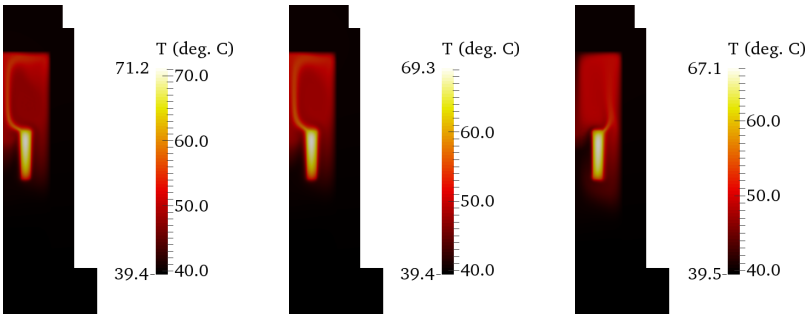


(a) Pure oil (b) Ferrofluid - $H = 0$ (c) Ferrofluid

Figure 11: Setup without core ($\phi = 7\%$ for (b) and (c)). Temperature field in the meridian plane at $t = 10000$s.

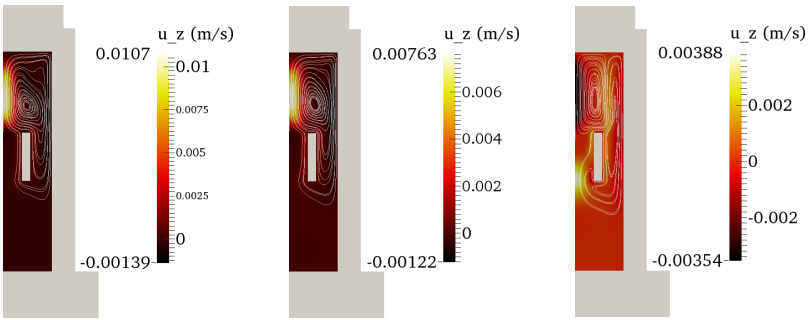


(a) Pure oil (b) Ferrofluid - $H = 0$ (c) Ferrofluid

Figure 12: Setup without core ($\phi = 7\%$ for (b) and (c)). Axial velocity field and streamlines in the meridian plane at $t = 10000$s.

the top and bottom spatial distributions of the velocity are almost symmetrical. These two convection cells enhance the cooling effect. Notice finally that the axial velocity is significantly higher when there is a ferromagnetic core.

We show in Fig. 15 the radial temperature profile at $z = 7.5$cm and $t = 10000$s. This height is that of the hot spot thermal sensor. One can clearly identify the core, coil, fluid and wall regions on the three curves shown in the figure. The plateaus correspond to the core and the wall. The temperature drop observed in the core when the pure oil is replaced by the ferrofluid and the Kelvin force switched off is about 2°C. The temperature drop is about 17°C when the Kelvin force is active in the fluid.

### *5.4. Maximum temperature and Nusselt number*

Fig. 16 shows the maximum temperature in the system at $t = 10000$s for all the volume fractions considered. The results shown in Fig. 16a correspond to the configuration without the ferromagnetic core, and the results shown in

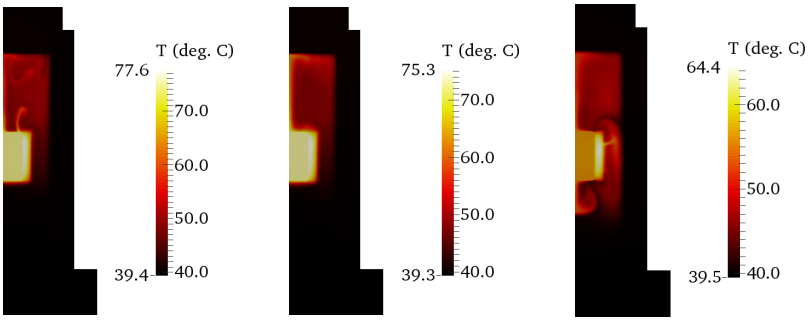


(a) Pure oil (b) Ferrofluid - $H = 0$ (c) Ferrofluid

Figure 13: Setup with core ($\phi = 7\%$ for (b) and (c)). Temperature field in a meridian plane at $t = 10000$s.

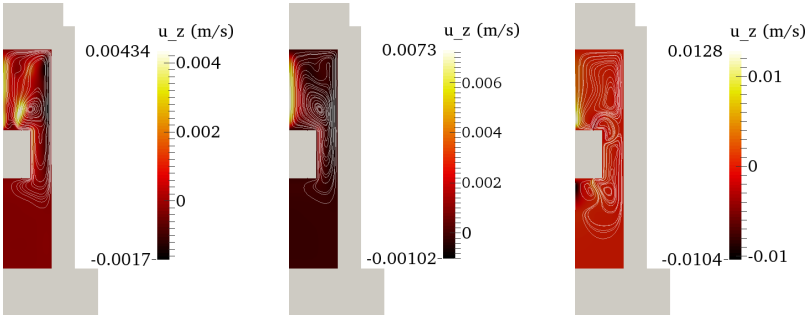


(a) Pure oil (b) Ferrofluid - $H = 0$ (c) Ferrofluid

Figure 14: Setup with core ($\phi = 7\%$ for (b) and (c)). Axial velocity field and streamlines in a meridian plane at $t = 10000$s.

Fig. 16b correspond to the configuration with the core. In each panel we compare the maximum temperature observed when the Kelvin force is active with the temperature observed when the Kelvin force is inactive. For both cases (core or not), the temperature decreases with the volume fraction. Also, for each concentration, the Kelvin force has a positive effect on the cooling. The thermomagnetic effect is stronger when the core is present.

The efficiency of thermal convection is usually characterized in the literature by a Nusselt number, which, in the present case, we define as follows:

$$N_u = \frac{T_{\max}^{\text{cond}} - T_0}{T_{\max}^{\text{conv}} - T_0}, \tag{22}$$

where $T_{\max}^{\text{cond}}$ is the maximum temperature in the system when considering only thermal conduction (the velocity is set to zero), and $T_{\max}^{\text{conv}}$ is the maximum temperature in the system when the convection is active. Fig. 17 shows the Nusselt number computed at $t = 10000$s for all the volume fractions considered.

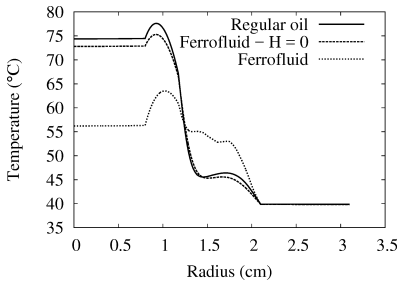


Figure 15: Setup with core (ferrofluid with $\phi = 7$ %). Temperature profile $T(r, z = 7.5$ cm) at $t = 10000$ s.

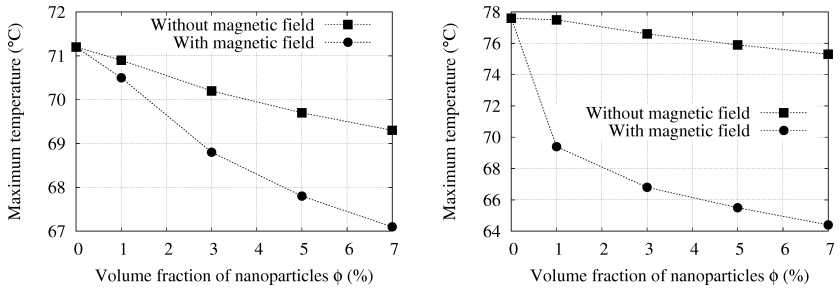


(a) Without core (b) With core

Figure 16: Maximum temperature in the system at $t = 10000$s as a function of the volume fraction of nanoparticles.

The results shown in Fig. 17a correspond to the configuration without the ferromagnetic core; the results shown in Fig. 17b correspond to the configuration with the core. Without the core, the Nusselt number decreases with the volume fraction, whether the Kelvin force is active or not. As expected though, for each concentration, the Nusselt number is larger when the Kelvin force is active. With core, we observe again that the Nusselt number is larger when the Kelvin force is active. The Nusselt number decreases as the volume fraction increases when the Kelvin force is switched off. The behavior of the Nusselt number is not monotone when the Kelvin force is active: it first increases until $\phi = 3\%$ and then decreases.

These graphs show again that the thermomagnetic convection improves the cooling of the solenoid by increasing the heat transfer rate. Notice that comparing the Nusselt numbers in the various configurations must be done with care: it may not be appropriate to estimate which configuration is the most efficient for heat transfers. For instance, without core and with the Kelvin force active, the Nusselt number at $\phi = 7\%$ is smaller than that at $\phi = 0\%$ whereas the cooling is more efficient (see Fig. 16a).

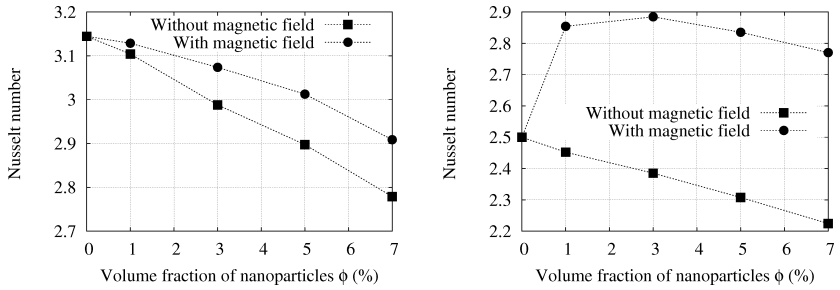


(a) Without core (b) With core

Figure 17: Nusselt number at $t = 10000$s as a function of the volume fraction of nanoparticles.

*5.5. Influence of the ferromagnetic core*

The core has two main effects on the heat transfer process: it blocks the upward motion of the flow close to the axis, and its high magnetic permeability ($\mu_r = 1000$) changes the magnetic field, therefore changing the Kelvin force.

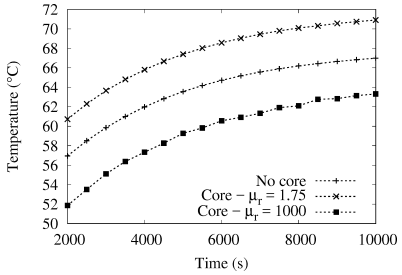


Figure 18: Ferrofluid cooling ($\phi = 7$ %). Effect of the core and its magnetic permeability on the time evolution of the temperature at the hot spot.

To discriminate the influence of these two effects, we set $\phi = 7$ % and we simulate the configuration with a core whose magnetic permeability is the same as that of the ferrofluid, i.e., $\mu_r \simeq 1.75$. The magnetic field that is generated in this situation is the same as that obtained with ferrofluid in the configuration without core. Hence, this situation only tests the blocking effect of the core.

Fig. 18 shows the effect of the core and its magnetic permeability on the temperature at the hot spot. The blocking effect of the core has a negative influence on the cooling performance; the temperature is about 4°C higher than in the configuration without the core at $t = 10000$ s. This confirms that blocking the flow in the core region reduces the heat transfer rate. When the magnetic permeability is that of iron ($\mu_r = 1000$), the cooling performance is increased: the temperature at the hot spot is about 8°C less than that obtained with $\mu_r = 1.75$. The blocking effect of the core is thus more than compensated by increasing the magnetic permeability from $\mu_r = 1.75$ to $\mu_r = 1000$.

Fig. 19 shows the effect of the core and its magnetic permeability on the magnetic field. As expected, the magnetic field in the configuration without

core is the same as in the configuration with a core with magnetic permeability $\mu_r = 1.75$. When $\mu_r = 1000$, the magnetic field gets stronger in the fluid region. This increased magnetic field creates the strong convection cells observed in Fig. 14c, which in turn enhances the cooling efficiency.

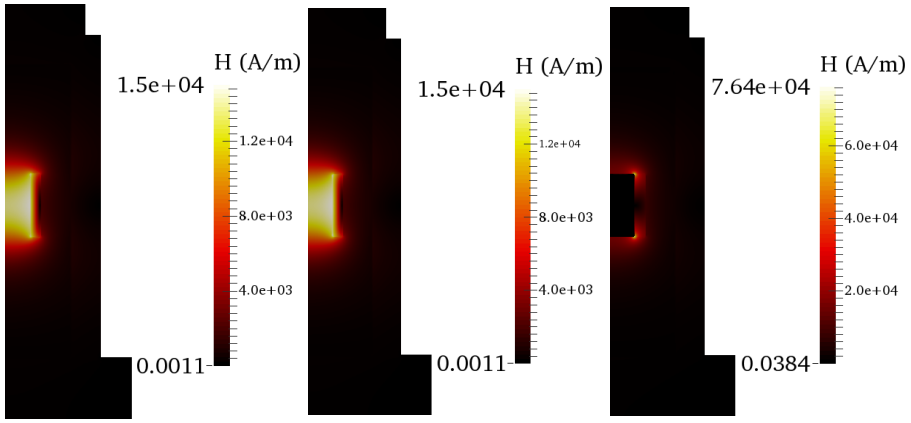


(a) No core (b) Core - $\mu_r = 1.75$ (c) Core - $\mu_r = 1000$

Figure 19: Ferrofluid cooling ($\phi = 7\%$). Effect of the core and its magnetic permeability on the magnetic field intensity.

Figure 20 shows the time evolution of the temperature drop at the hot spot between a case without Kelvin force and a case with the Kelvin force active for three configurations. The curve denoted as 'No core' corresponds to the case without core (see Fig. 11); the 'Core-$\mu_r = 1000$' curve corresponds to the case with a core whose magnetic permeability is 1000 (see Fig. 13); the 'Core-$\mu_r = 1.75$' curve corresponds to the case with a core whose magnetic permeability is 1.75. The temperature drop goes from about 2°C without core to 4°C with the $\mu_r = 1.75$ core and to about 12°C with the $\mu_r = 1000$ core. Consequently, the change in the magnetic permeability and the associated enhancement of the magnetic field have more impact on the temperature drop than the blocking effect of the core.

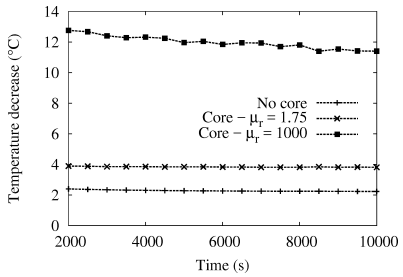


Figure 20: Ferrofluid cooling ($\phi = 7\%$). Effect of the core and its magnetic permeability on the temperature drop at the hot spot due to the Kelvin force.

## 6. Conclusions

We have numerically simulated the natural convection of a ferrofluid in a cylindrical container heated by a solenoid. The thermo-hydrodynamical model is first validated against an experiment using transformer oil. Simulations with different volume fractions of magnetic nanoparticles are then performed to observe the heat transfer effect of the properties of the ferrofluid and of the thermomagnetic convection. In order to make this work more representative of an electrical transformer, we have also studied the influence of a ferromagnetic core.

The ferrofluid appears to be an interesting cooling solution. The maximum temperature decreases as the volume fraction of nanoparticles increases. The heat transfers are increased by the presence of a ferromagnetic core. The Kelvin force significantly modifies the flow pattern whether there is a ferromagnetic core or not. The numerical results also demonstrate that the changes of the physical properties due to the nanoparticles significantly enhance the heat transfers. We have shown that the notion of Nusselt number must be used with care when comparing the cooling efficiency of the various configurations investigated in the present work. Finally, the high magnetic permeability of the core is shown to increase the magnetic field in the fluid region, causing a strenghtening of the cooling by thermomagnetic convection.

## Acknowledgement

This work was supported by the Labex LaSIPS (Nano-in-Oil Grant). The HPC resources for SFEMaNS were provided by GENCI-IDRIS (grant 2017-0254) in France and by the Texas A&M University Brazos HPC cluster. Support from the National Science Foundation under grants DMS 1620058, DMS 1619892 is acknowledged.

## References

[1] J. L. Neuringer, R. E. Rosensweig, Ferrohydrodynamics, Physics of Fluids 7 (12) (1964) 1927–1937.

[2] H. Yamaguchi, I. Kobori, Y. Uehata, K. Shimada, Natural convection of magnetic fluid in a rectangular box, Journal of Magnetism and Magnetic Materials 201 (1999) 264–267.

[3] S. M. Snyder, T. Cader, B. A. Finlayson, Finite element model of magnetoconvection of a ferrofluid, Journal of Magnetism and Magnetic Materials 262 (2003) 269–279.

[4] H. Yamaguchi, X.-R. Zhang, X.-D. Niu, K. Yoshikawa, Thermomagnetic natural convection of thermo-sensitive magnetic fluids in cubic cavity with heat generating object inside, Journal of Magnetism and Magnetic Materials 322 (2010) 698–704.

[5] P. S. B. Szabo, W.-G. Fürth, The transition from natural convection to thermomagnetic convection of a magnetic fluid in a non-uniform magnetic field, Journal of Magnetism and Magnetic Materials 447 (2018) 116–123.

[6] S. Odenbach, Magnetoviscous Effect in Ferrofluids, Springer, 2002.

[7] V. E. Fertman, L. E. Golovicher, N. P. Matusevich, Thermal Conductivity of Magnetite Magnetic Fluids, Journal of Magnetism and Magnetic Materials 65 (1987) 211–214.

[8] R. E. Rosensweig, Ferrohydrodynamics, Cambridge University Press, 1985.

[9] M. T. Krauzina, A. A. Bozhko, P. V. Krauzin, S. A. Suslov, The use of ferrofluids for heat removal: Advantage or disadvantage?, Journal of Magnetism and Magnetic Materials 431 (2017) 241–244.

[10] V. Segal, K. Raj, An investigation of power transformer cooling with magnetic fluids, Indian Journal of Engineering & Materials Science 5 (1998) 416–422.

[11] G.-Y. Jeong, S. P. Jang, H.-Y. Lee, J.-C. Lee, S. Choi, S.-H. Lee, Magnetic-Thermal-Fluidic Analysis for Cooling Performance of Magnetic Nanofluids Comparing With Transformer Oil and Air by Using Fully Coupled Finite Element Method, IEEE Transactions on Magnetics 49 (5) (2013) 1865–1868.

[12] L. Pîslaru-Danescu, A. M. Morega, M. Morega, V. Stoica, O. M. Marincia, F. Nouras, N. Paduraru, I. Borbàth, T. Borbàth, Prototyping a Ferrofluid-Cooled Transformer, IEEE Transaction on Industry Application 49 (3) (2013) 1289–1298.

[13] J. Patel, K. Parekh, R. V. Upadhyay, Prevention of hot spot temperature in a distribution transformer using magnetic fluid as a coolant, International Journal of Thermal Sciences 103 (2016) 35–40.

[14] J. Patel, K. Parekh, R. V. Upadhyay, Performance of Mn-Zn ferrite magnetic fluid in a prototype distribution transformer under varying loading conditions, International Journal of Thermal Sciences 114 (2017) 64–71.

[15] R. Zanella, C. Nore, F. Bouillault, L. Cappanera, I. Tomas, X. Mininger, J.-L. Guermond, Study of Magnetoconvection Impact on a Coil Cooling by Ferrofluid with a Spectral / Finite Element Method, IEEE Transaction on Magnetics 54 (2018) 1–4. doi:10.1109/TMAG.2017.2749539.

[16] J.-L. Guermond, R. Laguerre, J. Léorat, C. Nore, Nonlinear magnetohydrodynamics in axisymmetric heterogeneous domains using a Fourier/finite element technique and an interior penalty method, Journal of Computational Physics 228 (2009) 2739–2757.

[17] R. E. Rosensweig, Magnetic Fluids, Annual Reviews of Fluid Mechanics 19 (1987) 437–463.

[18] J. Eapen, R. Rusconi, R. Piazza, S. Yip, The Classical Nature of Thermal Conduction in Nanofluids, Journal of Heat Transfer 132 (102402) (2010) 1–14.

[19] A. Vatani, P. L. Woodfield, D. V. Dao, A survey of practical equations for prediction of effective thermal conductivity of spherical-particle nanofluids, Journal of Molecular Liquids 211 (2015) 712 – 733.

[20] W. T. Perrins, D. R. McKenzie, R. C. McPhedran, Transport properties of regular arrays of cylinders, Proceedings of the Royal Society of London. Series A, Mathematical and Physical Sciences 369 (1737) (1979) 207–225.

[21] S. Balay, S. Abhyankar, M. F. Adams, J. Brown, P. Brune, K. Buschelman, V. Eijkhout, W. D. Gropp, D. Kaushik, M. G. Knepley, L. C. McInnes, K. Rupp, B. F. Smith, H. Zhang, PETSc users manual, Tech. Rep. ANL-95/11 - Revision 3.5, Argonne National Laboratory (2014).

[22] A. Bonito, J.-L. Guermond, F. Luddens, Regularity of the Maxwell equations in heterogeneous media and Lipshitz domains, Journal of Mathematical Analysis and Applications 408 (2013) 498–512.

[23] C. Nore, H. Zaidi, F. Bouillault, A. Bossavit, J.-L. Guermond, Approximation of the time-dependent induction equation with advection using Whitney elements, COMPEL: The International Journal for Computation and Mathematics in Electrical and Electronic Engineering 35 (1) (2016) 326–338.

[24] A. Giesecke, C. Nore, F. Stefani, G. Gerbeth, J. Léorat, W. Herreman, F. Luddens, J.-L. Guermond, Influence of high-permeability discs in an axisymmetric model of the Cadarache dynamo experiment, New Journal of Physics 14 (053005) (2012) 1–16.

[25] T. L. Bergman, A. S. Lavine, F. P. Incropera, D. P. Dewitt, Fundamentals of Heat and Mass Transfer, John Whiley & Sons, USA, 2011.